PHOTONICS Research

Broadband rhenium disulfide optical modulator for solid-state lasers

Xiancui Su,[1] Baitao Zhang,[1,*] Yiran Wang,[1] Guanbai He,[1] Guoru Li,[1] Na Lin,[1] Kejian Yang,[1] Jingliang He,[1,3] and Shande Liu[2]

[1]State Key Laboratory of Crystal Materials, Shandong University, Jinan 250100, China
[2]College of Electronics, Communication, and Physics, Shandong University of Science and Technology, Qingdao 266590, China
[3]e-mail: jlhe@sdu.edu.cn
*Corresponding author: btzhang@sdu.edu.cn

Received 19 February 2018; revised 6 March 2018; accepted 7 March 2018; posted 7 March 2018 (Doc. ID 324505); published 26 April 2018

Rhenium disulfide (ReS_2), a member of group VII transition metal dichalcogenides (TMDs), has attracted increasing attention because of its unique distorted 1T structure and electronic and optical properties, which are much different from those of group VI TMDs (MoS_2, WS_2, $MoSe_2$, WSe_2, etc.). It has been proved that bulk ReS_2 behaves as a stack of electronically and vibrationally decoupled monolayers, which offers remarkable possibilities to prepare a monolayer ReS_2 facilely and offers a novel platform to study photonic properties of TMDs. However, due to the large and layer-independent bandgap, the nonlinear optical properties of ReS_2 from the visible to mid-infrared spectral range have not yet been investigated. Here, the band structure of ReS_2 with the introduction of defects is simulated by the *ab initio* method, and the results indicate that the bandgap can be reduced from 1.38 to 0.54 eV with the introduction of defects in a suitable range. In the experiment, using a bulk ReS_2 with suitable defects as the raw material, a few-layered broadband ReS_2 saturable absorber (SA) is prepared by the liquid phase exfoliation method. Using the as-prepared ReS_2 SA, passively *Q*-switched solid-state lasers at wavelengths of 0.64, 1.064, and 1.991 μm are investigated systematically. Moreover, with cavity design, a femtosecond passively mode-locked laser at 1.06 μm is successfully realized based on the as-prepared ReS_2 SA for the first time. The results present a promising alternative for a rare broadband optical modulator and indicate the potential of ReS_2 in generating *Q*-switched and mode-locked pulsed lasers. It is further anticipated that this work may be helpful for the design of 2D optoelectronic devices with variable bandgaps.

OCIS codes: (160.4330) Nonlinear optical materials; (140.3540) Lasers, Q-switched; (140.3580) Lasers, solid-state; (140.4050) Mode-locked lasers; (160.4236) Nanomaterials.

https://doi.org/10.1364/PRJ.6.000498

1. INTRODUCTION

Recently, 2D materials, including graphene [1], topological insulators (Bi_2Se_3, Bi_2Te_3, etc.) [2–5], black phosphorus [6–10], and transition metal dichalcogenides (TMDs) (MoS_2, WS_2, etc.) [11,12], with outstanding electronic and optical properties have been widely used in energy storage devices, transistors, photodetectors, electroluminescent devices, and optical saturable absorbers for ultrafast photonics [13–28]. Among these materials, 2D TMDs are relatively easy to exfoliate, affordable, and highly reliable [29–31]. Further, 2D TMDs are materials consisting of an atomic plane of a transition metal (Mo, W, Re, Ti, Zr, Hf, V, Nb, Ta, etc.) sandwiched between two chalcogen planes (S, Se, Te) [32,33]. Aside from the most popular TMDs of group VI (MoS_2, WS_2, $MoSe_2$, WSe_2, etc.), ReS_2, a representative of group VII TMDs, has recently attracted significant interest for its unusual properties in many aspects of structural, electro-optical, and chemical properties [34,35]. A vision has emerged that ReS_2 will apparently be more worthwhile over isotropic TMDs from group VI for traditional applications and beyond. Differing from the popular group VI TMDs, due to charge decoupling from an extra valence electron of Re atoms, ReS_2 possesses a unique distorted 1T structure with weak interlayer coupling, which offers remarkable possibilities to prepare few-layered ReS_2 facilely [36]. As a result of the distorted 1T structure, both the monolayer and bulk ReS_2 are direct bandgap semiconductors. Furthermore, the overall bandgap does not change significantly from monolayer to multilayer (1.35 eV for bulk and 1.43 eV for monolayer) [37]. Consequently, ReS_2 has shown layer-independent electrical, optical, and vibrational properties [38]. This suggests that ReS_2 could offer a novel platform to study mesoscopic physics of 2D systems without the limitation of obtaining monolayer-thick flakes. However, the large and layer-independent bandgap also causes a problem for applications where a particular bandgap is required. For 2D materials, it

has been reported that the impurities or defects in materials can localize electronic states, which in turn can generate narrow bands, a Mott transition, and even Anderson localization [39]. Recently, the existence of lattice imperfections in 2D graphene-like structures has been used to tail local properties and achieve new functionality [40,41]. Inspired by this conclusion, in this work, we calculated the band structure with the introduction of defects by the *ab initio* method [15]. The result shows that the bandgap of ReS_2 reduces with the modification of S defects. We believe this work may be helpful in the design of variable bandgaps in 2D optoelectronic materials.

In the past years, there has been observed a growing interest in fundamental and applied research related to ReS_2 [36,42]. Among these achievements, the nonlinear optical properties and the corresponding applications are rarely investigated, in contrast with its electronic and chemical properties. Recently, Liu *et al.* and Mao *et al.* have found ReS_2 can be used in 1.5 μm fiber lasers as the saturable absorber (SA) and obtained picosecond pulse lasers [43,44]. In comparison with fiber lasers, solid-state lasers possess superiorities, such as high power and smooth spectral property without sidebands. Recently, our group has achieved a *Q*-switched solid-state laser at 2.8 μm by using ReS_2 as a saturable absorber [45]. The above successful applications in ultrafast lasers make ReS_2 a promising optical modulator. However, the mechanism that the ReS_2 with a large bandgap (~1.35 eV) can be used at a wavelength beyond the theoretical response wavelength (shorter than 0.918 μm) still lacks verification in both theory and experiment. In addition, up to now, the broadband absorption properties and the applications in solid-state lasers have not been investigated systematically. In this paper, based on the theoretical analysis, by using bulk ReS_2 with suitable S defects as raw material, a broadband ReS_2 SA is constructed, and its properties are characterized systematically. Using the as-prepared ReS_2 SA in solid-state lasers, passively *Q*-switched lasers at 0.64, 1.064, and 1.991 μm are demonstrated, respectively. To further study their ability to generate ultrafast pulses, their ultrafast photonics application in a femtosecond solid-state laser is realized successfully for the first time, to the best of our knowledge, and pulses as short as 323 fs were obtained at 1.06 μm with an output power of 350 mW. The above work broadens the applied spectral ranges of ReS_2 and experimentally identifies that ReS_2 with suitable S defects is a promising broadband optical modulator.

2. THEORETICAL ANALYSIS OF THE BAND STRUCTURE

Based on the reported unit-cell parameter of ReS_2, the monolayer supercell with 36 Re atoms and 72 S atoms is created and optimized by using the Vienna *ab initio* simulation package [46]. The calculated band structures with different Re to S ratio (*R*) are shown in Fig. 1. When *R* is 1∶2, from Fig. 1(b), it can be seen that ReS_2 is a direct gap semiconductor with a bandgap of 1.38 eV, which is close to the experimental value of 1.37 eV [47]. With S atomic defects, the band structures of monolayer ReS_2 are calculated with *R* of 1∶1.972, 1∶1.944, and 1∶1.889, respectively, as shown in Figs. 1(c)–1(e). The results show that the bandgap of ReS_2 decreases with the increase of S vacancies. However, when Re vacancies are introduced, electrons are localized near the S atoms, which are close to the Re vacancies, which results in the non-negligible electronic density of states at the Fermi level. As shown in Fig. 1(a), by introducing Re vacancy with *R* of 1∶2.057, the energy band intersects with the Fermi level, which indicates that, in this case, the ReS_2 has no bandgap and exhibits a metallic character. The above results show that S-containing defects result in a small but noticeable reduction of the bandgap, whereas Re-containing defects work adversely, which is comparable with the results of WS_2 and MoS_2 [41,48]. A difference is that the creation of an Re vacancy causes the character of ReS_2 from semiconductor to metallic state, while WS_2 and MoS_2 retain semiconductors with a W or Mo vacancy. It appears that, due to the complex distorted 1T structure of ReS_2, the electronic localization in a ReS_2 monolayer is more severe, as compared with the MoS_2 and WS_2 monolayer case.

Based on the calculation results, it can be concluded that, by the introduction of S defects in a suitable range, the bandgap of ReS_2 can be reduced from 1.38 ($R = 1:2$) to 0.56 eV ($R = 1:1.889$), and the corresponding absorption wavelength edge extends from 0.9 to 2.2 μm. Due to the layer-independent properties of ReS_2, the above calculations based on a monolayer ReS_2 should be effective for multilayer and bulk ReS_2. Considering the semiconducting properties of ReS_2, when ReS_2 is excited by light with photon energy larger than the gap energy, electrons will be transferred from the valance band to the conduction band. Under strong excitation, the final states will be fully occupied and exhibit saturable absorption, which indicates that ReS_2 with S defects can be used as a broadband saturable absorber [41].

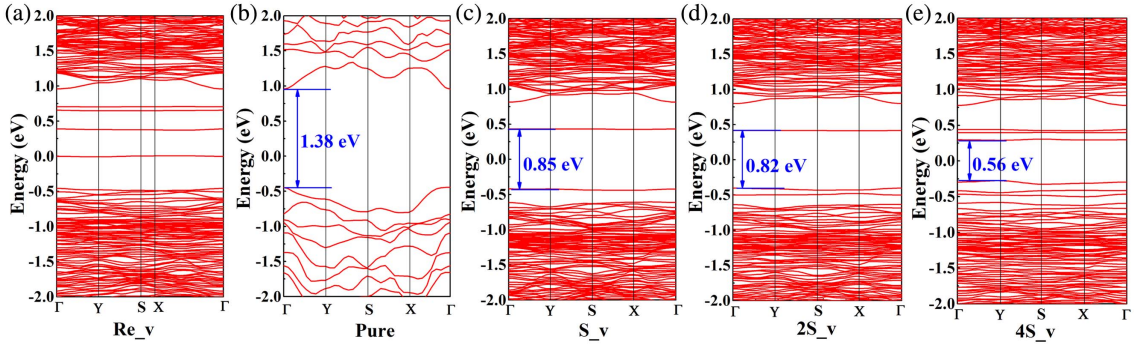

Fig. 1. Theoretical band structure of monolayer ReS_2. (a) $R = 1:2.057$, (b) $R = 1:2$, (c) $R = 1:1.972$, (d) $R = 1:1.944$, and (e) $R = 1:1.889$.

3. PREPARATION AND CHARACTERIZATION OF THE ReS_2 SA

For ReS_2 SA preparation, the liquid phase exfoliation (LPE) is considered as a simple but effective technique to synthesize ReS_2 from the bulk crystals toward few-layered structures. First, the ReS_2 powder was prepared from bulk crystal through a grinding process. Then, we mixed the ReS_2 powder with alcohol and executed 4-h ultrasonic exfoliation to undertake the liquid exfoliation process. To avoid the change of the material properties under high temperature, the ultrasonic process was operated at a suitable interval. After that, the solution was centrifuged at 2000 r/min for 10 min and the supernatant was collected for standby. Finally, the extracted ReS_2 supernatant was transferred onto a plane substrate or mirror by spin coating at 500 r/min for 10 s and dried under an infrared oven lamp. Recent studies have shown that controllable formation of vacancies in monolayer TMDs can be realized experimentally by the methods such as pulsed laser deposition (PLD), α-particle irradiation, and thermal annealing [41,49]. Most of the above methods control the defects by tuning the ratio of the atoms in raw materials. However, the various growth conditions, proton thermal motion, and mechanical stress also can cause lattice imperfection, which makes it difficult to control the defects of the SA precisely. In this work, based on the theoretical analysis, by characterization with energy-dispersive X-ray spectroscopy (EDS), we chose a commercially available purity ReS_2 bulk crystal with suitable defects as the raw material. With the EDS, the *R* of the bulk ReS_2 is characterized by point scanning and map scanning, respectively. In the point scanning, we selected 12 points randomly on the surface of ReS_2 sample, and the result shows that the *R* ranges from 1∶1.828 to 1∶1.919 by moving from the center to the edge of the sample. To confirm the average ratio, as shown in the inset of the Fig. 2(a), the bulk ReS_2 sample is placed on a piece of carbon conductive adhesive, and a 4 mm × 3 mm area is measured by map scanning. Except for the C atoms and O atoms from air and the conductive adhesive, the average *R* is 1∶1.846 for the bulk sample, which matches well with the ratio range measured by point scanning. After the exfoliation process, to identify the existence of vacancies in the as-prepared ReS_2 SA, we measure the average *R* of the few-layered ReS_2 SA based on the sapphire substrate. As shown in Fig. 2(b), except for the C, O, and Al from air and the sapphire substrate, the average *R* of the ReS_2 flakes is measured to be 1∶1.743. Compared with the bulk ReS_2, the proportion of S atoms reduces in the few-layered ReS_2 SA. This is because, during the preparation of ReS_2 SA, especially in the process of grinding and ultrasonic exfoliation, some defects or vacancies are introduced at the Re sites and S sites under the action of external forces. In the structure of ReS_2, S atoms located on the out-of-plane [27]. Thus, in the process of exfoliation, compared with Re atoms, more S atoms are replaced by vacancies or defects due to atomic collision. As a consequence, the *R* of bulk ReS_2 is different from that of few-layered flakes. According to the theoretical analysis, the bandgap of ReS_2 reduces with the S vacancies. Therefore, the sample has a bandgap less than 0.56 eV, and the corresponding maximum absorption wavelength should be greater than 2.2 μm.

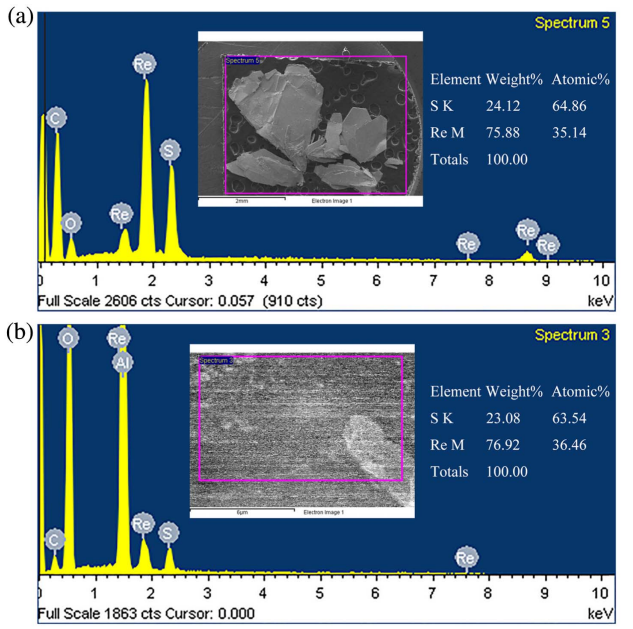

Fig. 2. Measured position and the corresponding EDS image of (a) the raw bulk ReS_2 and (b) the as-prepared few-layered ReS_2.

To identify the thickness and the distribution of the flakes, an atomic force microscope (AFM) is used to study the morphology of the as-prepared ReS_2 SA. Figure 3(a) shows an AFM scan image of the sample in a large area, due to the weak interlayer coupling, where the distribution of flake thicknesses, as shown in Fig. 3(b), indicates good uniformity of the flake thickness. To study the detailed morphology, a smaller area is measured with high resolution, as shown in Fig. 3(c). The length and width of ReS_2 flakes are as large as 3–5 μm, which has potential for applications in solid-state bulk lasers, where the

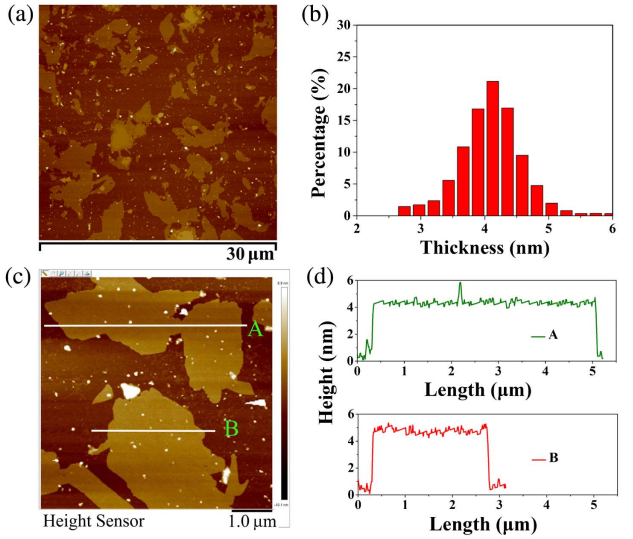

Fig. 3. (a), (b) AFM image of the ReS_2 SA with 30 μm × 30 μm area and the corresponding distribution of flake thicknesses. (c), (d) High-resolution AFM image with 6 μm × 6 μm area and the typical height profiles.

oscillation laser dimension is much larger than it is in fiber lasers. Compared with the samples in our previous paper, the flakes in this work have a slightly larger dimension and thickness [45]. That is because, in the two preparation processes, the concentration of ReS_2 and the ultrasonic time differ, resulting in a slight difference in thickness and dimension of the flakes. Figure 3(d) shows the typical height profiles of the section marked in Fig. 3(c). The thickness of the flakes is about 4 nm, corresponding to ~6 layers thick [50].

The Raman spectra of the as-prepared ReS_2 SA and the pure sapphire substrate are measured by a Raman microscope with a 532 nm laser as the excitation source, as shown in Fig. 4(a). The Raman spectrum was acquired in the 100–500 cm^{-1} wavenumber range by a lens-based spectrometer with a cooled charge-coupled device (CCD) detector. A 100×, NA = 0.9 objective is used to focus the beam on the flake with 1.0 μm diameter. The spectral resolution of the setup was 0.34 cm^{-1} per CCD pixel for an 1800 grooves/mm grating. In general, there are two types of active Raman modes in 2D ReS_2, intralayer vibration modes (higher frequencies) and interlayer vibration modes (lower frequencies) [29]. However, due to the weak lattice coupling between the layers, these low-frequency vibrational modes are usually quite challenging to be observed. Thus, Fig. 4(a) only shows the typical intra-layer vibration modes to confirm the material as ReS_2. The A_g modes located at 137.1 and 143.7 cm^{-1} are assigned to out-of-plane vibrations of Re atoms. Among the E_g modes, the modes located at 151.8, 162.4, 213.2, and 235.5 cm^{-1} are caused by the in-plane vibrations of Re atoms, while the modes located at 307.1 and 310.7 cm^{-1} are due to the in-plane vibrations of S atoms [51]. Except for these modes, due to the low symmetry of ReS_2, there are many higher-frequency Raman modes in Fig. 4(a), which are mainly coming from the light S atoms.

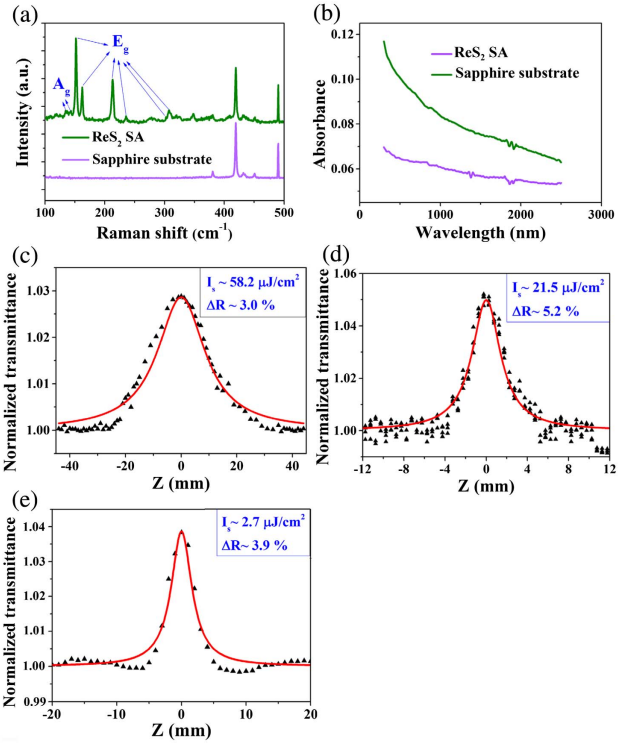

Fig. 4. (a) Raman spectra of the ReS_2 SA and the sapphire substrate. (b) Absorption spectra of the ReS_2 SA and the sapphire substrate, respectively. (c)–(e) Open aperture Z-scan curves of the ReS_2 SA at 0.73, 1.06 and 1.94 μm, respectively.

As shown in Fig. 4(b), the absorbance spectra of the ReS_2 SA and the pure sapphire substrate are measured using a U-3500 Hitachi UV/VIS/NIR spectrophotometer. It clearly shows that the ReS_2 sample has smooth absorption in the ultraviolet to mid-infrared wavelength bands, which demonstrates that the ReS_2 SA might be a promising broadband optical material. The Z-scan technique is used to investigate the nonlinear optical response of the as-prepared few-layered ReS_2 [52]. The experiment setup has been widely described in a previous report [25]. For the pump source, three stable mode-locked lasers at 0.73 μm (pulse duration: 120 fs; repetition rate: 79.7 MHz), 1.06 μm (pulse duration: 15 ps; repetition rate: 41.54 MHz), and 1.94 μm (pulse duration: 1.8 ps; repetition rate: 87.73 MHz) were used, respectively. Due to the limitation of the experiment conditions, the wavelengths of the pump sources do not match the laser output wavelengths, but the results still can show the broadband SA properties of the sample from the visible to infrared band. Figures 4(c)–4(e) show the measured open aperture Z-scan curves of the ReS_2 SA at 0.73, 1.06, and 1.94 μm, respectively. The normalized transmittance gradually increases when the ReS_2 sample moves toward the focus point ($Z = 0$), indicating that the absorption of few-layered ReS_2 flakes becomes saturated with the increase of the incident pump intensity. This process is well-known as the typical saturable absorption behavior. The saturable absorption process could be studied by the analysis model of a two-level saturable absorber, and the intensity-dependent transmission formula is described as [25]

$$T = \left[1 - \frac{\alpha_0 L I_s}{I_s + I_0/(1 + Z^2/Z_0^2)}\right] \Big/ (1 - \alpha_0 L), \quad (1)$$

where T is the normalized transmittance of the sample, L is the sample length, $\alpha_0 L$ is the modulation depth of the sample, I_0 is the peak intensity, Z_0 is the diffraction length of the beam, and I_s is the saturation intensity. Using Eq. (1) to fit the measured data, for 0.73, 1.06, and 1.94 μm, the saturable intensities are determined to be 58.2, 21.5, and 2.7 $\mu J/cm^2$, and the modulation depths are 3%, 5.2%, and 2.9%, respectively. Combined with the broadband absorption spectrum in Fig. 4(b), the existence of saturable absorption further makes the as-prepared ReS_2 SA as a broadband optical modulator possible.

4. VISIBLE, NEAR-INFRARED, AND MID-INFRARED *Q*-SWITCHED LASERS WITH A ReS_2 SA

With a compact 3 cm long two-mirror resonator, passively *Q*-switched solid-state lasers based on the as-prepared ReS_2 SA around 0.64, 1.064, and 1.991 μm bands are investigated with Pr:YLF, Nd:YAG, and Tm:YAP as gain media, respectively. The transmittance of the three output couplers (OCs) were 1%, 10%, and 5% for 0.64, 1.064, and 1.991 μm,

respectively. For 0.64 μm, the input mirror (IM) was plane and the OC had a radius of curvature of 100 mm. For 1.064 μm, the IM and OC were both plane mirrors. For the 1.991 μm laser, the IM had a radius of curvature of 1000 mm and the OC was plane. By continuously increasing the pump power and finely tilting the ReS_2 SA, a nicely *Q*-switched pulse laser can be easily achieved. The average output power, peak power, pulse duration, and repetition rate versus the absorbed pump power at 0.64, 1.064, and 1.991 μm are shown in Figs. 5(a)–5(f), respectively. From the figure, we can see the output power and repetition rate increase with the absorbed pump power, while the pulse duration decreases, which are typical results of passively *Q*-switched lasers. We stopped increasing the pump power when the output pulse trains became unstable. Under the maximum absorbed pump power, the pulse trains and the corresponding output spectra at the wavelengths of 0.64, 1.064, and 1.991 μm are shown in Figs. 6(a)–6(f), respectively. Limited to our experimental conditions, the optical spectrum analyzer (AvaSpec-NIR256) with the resolution of 3.7 nm is the only equipment that can measure the laser spectra ranging from the visible to mid-infrared band. Due to the low resolution of 3.7 nm, the spectra look smooth and cannot show the precise full width at half-maximum (FWHM). Thus, the laser output spectra cursorily measured in Fig. 6 are only to characterize the laser output wavelength. The detailed output parameters under the maximum absorbed pump power are shown in Table 1. The shortest pulse durations at 0.64, 1.064, and 1.991 μm are 160, 139, and

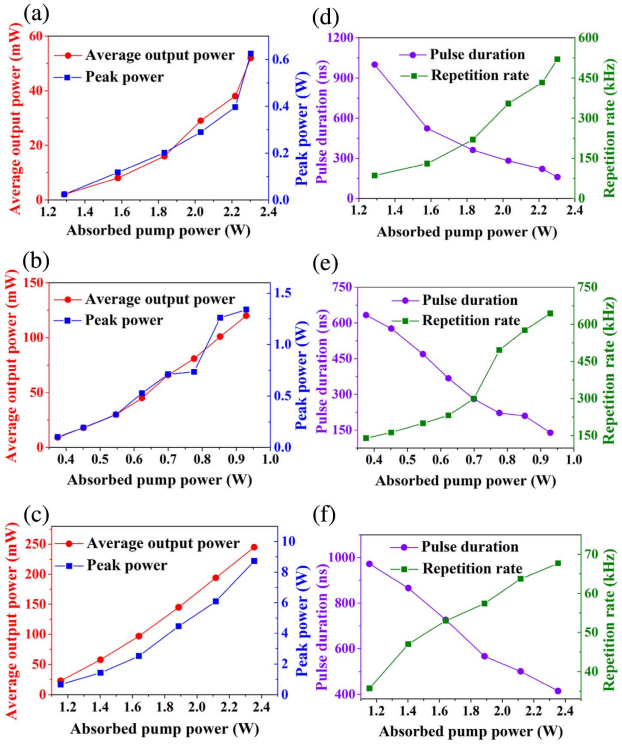

Fig. 5. ReS_2 *Q*-switched laser characteristics. (a)–(c) Average output power and peak power versus the absorbed pump power at 0.64, 1.064, and 1.991 μm, respectively. (d)–(f) Pulse duration and repetition rate versus the absorbed pump power at 0.64, 1.064, and 1.991 μm, respectively.

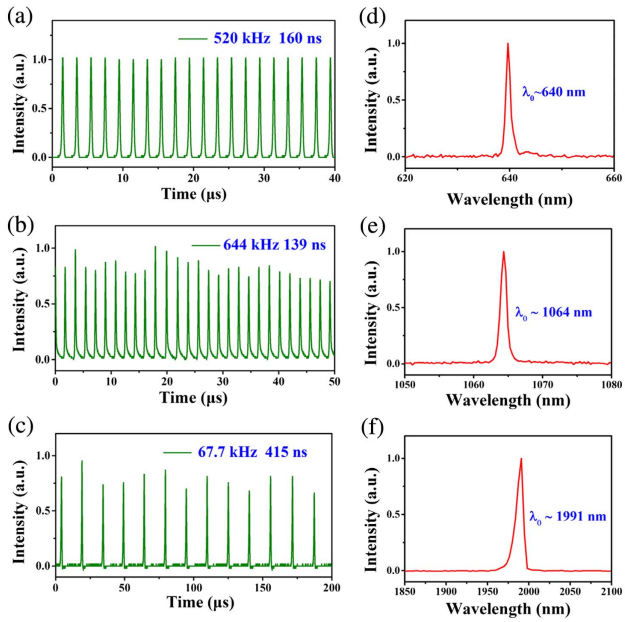

Fig. 6. (a)–(c) Recorded pulses trains of the ReS_2-based *Q*-switched lasers at 0.64, 1.064, and 1.991 μm, respectively. (d)–(f) Measured output spectra of the ReS_2-based *Q*-switched lasers at 0.64, 1.064, and 1.991 μm, respectively.

415 ns, respectively, which are fairly nice results for 2D-materials-based *Q*-switched lasers. The instabilities (output power, rms) for 0.64, 1.064, and 1.991 μm are measured to be 1.529%, 2.477%, and 2.318% at 0.5 h, respectively. For passively *Q*-switched lasers, many factors contribute to the instability of the pulse, such as the spatial hole burning affected by the crystal length, cavity length, and the crystal position in laser cavity, the absorption cross-section of the saturable absorber, and the gain cross-section of the gain medium. In our *Q*-switching experiments, the gain media, the radii of the input mirrors and output mirrors, the transmittance of the mirrors, and the initial transmissions of SA for different wavelengths are all different, which causes the different stabilities of the three lasers. Compared with the 1.064 and 1.991 μm lasers, the smaller laser mode radius on the SA, larger reflectivity of the output mirror, and higher absorbance of SA in the visible laser are conducive to the result that the pulse train of the visible *Q*-switched laser is more uniform than those of the other two [53].

With the relationship between intracavity power and the output power, the intracavity energy intensity I on the SA can be calculated by the following formula:

Table 1. Results of the Passively *Q*-Switched Lasers Based on the ReS_2 SA

	Visible	Near-Infrared	Mid-Infrared
Wavelength (nm)	640	1064	1991
Average output power (mW)	52	120	245
Repetition rate (kHz)	520	644	677
Pulse duration (ns)	160	139	415
Peak power (W)	0.625	1.34	8.72

$$I = \frac{\bar{P}_{\text{out}}}{f} \cdot \frac{1 + R_{\text{oc}}}{1 - R_{\text{oc}}} \cdot \frac{1}{\pi r^2}, \quad (2)$$

where $\bar{P}_{\text{out}}$ is the average output power, f is the repetition rate, R_{oc} is the reflection of the output mirror, and r is the radius of the oscillating laser mode on the SA. Based on the ABCD matrix, the r in the lasers at 0.64, 1.064, and 1.991 μm are 90, 130, and 170 μm, respectively. Thus, the corresponding maximum intracavity energy intensities on the ReS_2 are 78.3, 6.7, and 15.6 mJ/cm^2, respectively. In the experiments, no optical damage or degradation of laser performance is observed, even at the highest available fluence. Additionally, because the optical damage threshold is relative to the pulse width and in direct proportion to wavelength, the optical damage threshold of ReS_2 should be larger than 78.3 mJ/cm^2 for the nanosecond pulsed lasers at the wavelengths longer than 0.64 μm.

5. ULTRAFAST LASER WITH A ReS_2 SAM

To further study the saturable absorption of ReS_2 and investigate its ability to generate ultrafast pulses, its application in a mode-locked solid-state laser is studied. We choose Yb:CALGO as a gain medium for its excellent properties, such as the wide and smooth emission spectrum and high thermal conductivity [54]. Based on the ABCD propagation matrix method, the ReS_2-based mode-locked laser is built in a 2.96 m long z-type resonator, as shown in Fig. 7. The laser modes radii are calculated as 50 μm and 60 μm on Yb:CALGO and ReS_2, respectively. To precisely control the oscillating spot size on the ReS_2 in the mode-locked laser, here, the as-prepared ReS_2 supernatant is directly spin-coated on a mirror with high-reflection (HR) coating at 1020–1100 nm as the ReS_2 saturable absorption mirror (SAM).

With the ReS_2 SAM used in the cavity, after careful adjustment, the laser runs into a continuous wave mode-locked (CWML) regime when the absorbed pump power exceeds 5.13 W. Figure 8(a) shows the dependence of average output power versus the absorbed pump power. Under the absorbed pump power of 6.47 W, a maximum average output power of 350 mW is obtained, which is hundreds of times higher than those from ReS_2-based fiber lasers [43,44]. The instabilities (output power, rms) are measured to be less than 2% at 1 h. Figure 8(b) shows the pulse trains in 500 ns and 100 μs time scale at the maximum output power. As shown in Figs. 9(a) and 9(b), the pulse duration is measured to be 323 fs by sech^2 pulse shape fitting, and the spectrum is centered at 1060 nm with an

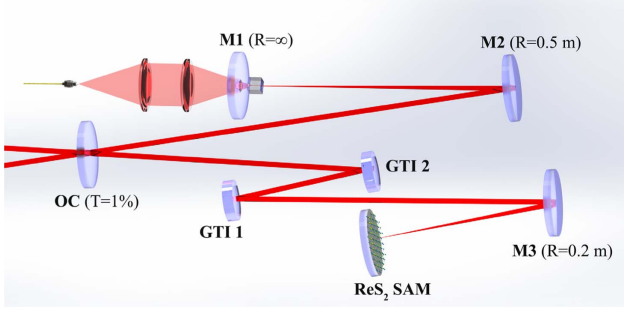

Fig. 7. Experimental setup of the ReS_2-based mode-locked laser.

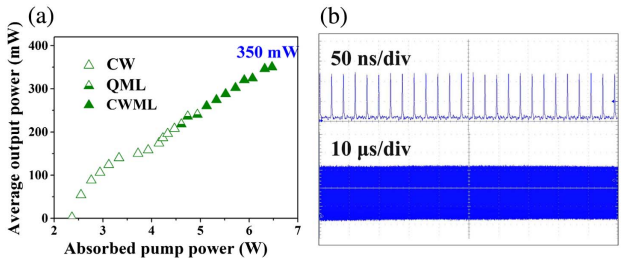

Fig. 8. (a) Average output power versus the absorbed pump power of the ReS_2-based mode-locked laser. (b) Recorded CWML pulse trains under the maximum pump power.

FWHM of 4.23 nm, corresponding to the time bandwidth product of 0.365. In addition, the recorded radio frequency spectrum is shown in Fig. 9(c), with a fundamental beat note near 50.7 MHz and the corresponding signal-to-noise ratio of 60 dB, which is measured by a spectrum analyzer (Agilent N9000A) with resolution bandwidth (RBW) of 10 kHz. Figure 9(d) is recorded in a wide span of 1 GHz with RBW of 1.0 MHz, and the absence of any spurious modulation proves clean CWML operation of ReS_2 mode-locked laser.

A mode-locked laser requires harsh conditions, so, besides mode matching on the gain material, a suitable energy intensity relative to the saturation fluence of the SA is a key factor. It is worth noting that, during the experiment, only a partial region of the ReS_2 SAM is available to support the mode-locking generation. One of the reasons is that, prepared by the simple LPE method, the ReS_2 flakes cannot distribute uniformly on the surface of the mirror. As a result, the sample shows a low surface-finish quality. In addition, based on the EDS analysis of the few-layered ReS_2, the ReS_2 flakes showed various bandgap as the probe location on the ReS_2 sample changed. For a mode-locked laser with a complex cavity, the above factors are of great importance to the establishment and stabilization of the mode-locked laser.

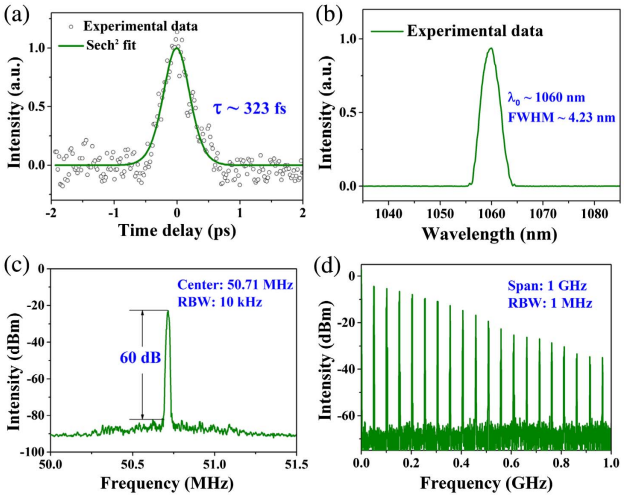

Fig. 9. Recorded results of ReS_2-based mode-locked laser. (a), (b) Autocorrelation trace for 323 fs duration and the corresponding spectrum. (c), (d) Recorded frequency spectrum with a narrow and a wide span, respectively.

For laser pulses longer than a few tens of picoseconds, the intense radiation brings heat deposition in the lattice, which finally causes dielectric breakdown and thermal damage. However, for ultrafast pulses shorter than 10 ps, the extremely high peak power directly breaks chemical bonds of the materials. Therefore, the damage threshold for femtosecond lasers should be evaluated with peak power intensity rather than energy intensity. In the CWML operation, the maximum peak power intensity on the SA is 18.7 GW/cm^2, and there is no damage observed, which indicates the damage threshold of ReS_2 for femtosecond laser should be larger than 18.7 GW/cm^2. However, until the laser turned into CWML, the laser operated in an unstable *Q*-switched mode-locking regime when some damage occurred due to the abruptly jumped pulses with extremely high peak power.

6. CONCLUSION

We calculate the band structure of ReS_2 with different ratios of Re and S by Vienna *ab initio* simulations and find that the bandgap reduces with the S defects. In experiments, we prepared a broadband few-layered ReS_2 SA with the LPE method, and the characterizations indicated its broadband saturable absorption properties from the visible to mid-infrared wavelengths. Using the as-prepared ReS_2 SA, passively *Q*-switched lasers at 0.64, 1.064, and 1.991 μm were realized, respectively. To further study the saturable absorption and its application in ultrafast photonics, a femtosecond solid-state laser based on few-layered ReS_2 was achieved successfully for the first time, and pulses as short as 323 fs were obtained at 1.06 μm with an output power of 350 mW. Our results highlight that ReS_2 with suitable S defects is a promising alternative for a rare broadband optical modulator and indicate the potential of ReS_2 in generating *Q*-switched and mode-locked pulsed lasers. Recent studies have shown that controllable formation of vacancies in monolayer TMDs can be realized experimentally by pulsed laser deposition, α-particle irradiation, and thermal annealing. Combining with these techniques, we believe that our work will be helpful for the design of ReS_2 optoelectronic devices with variable bandgaps.

Funding. National Natural Science Foundation of China (NSFC) (51321091, 61505098, 61575110, 61675116); Young Scholars Program of Shandong University (SDU) (2017WLJH48).

REFERENCES

1. A. K. Geim and K. S. Novoselov, "The rise of graphene," Nat. Mater. **6**, 183–191 (2007).
2. J. E. Moore, "The birth of topological insulators," Nature **464**, 194–198 (2010).
3. M. Z. Hasan and C. L. Kane, "Colloquium: topological insulators," Rev. Mod. Phys. **82**, 3045–3067 (2010).
4. Y. Chen, C. Zhao, S. Chen, J. Du, P. Tang, G. Jiang, H. Zhang, S. Wen, and D. Tang, "Large energy, wavelength widely tunable, topological insulator Q-switched erbium-doped fiber laser," IEEE J. Sel. Top. Quantum Electron. **20**, 0900508 (2014).
5. Y. Chen, C. Zhao, H. Huang, S. Chen, P. Tang, Z. Wang, S. Lu, H. Zhang, S. Wen, and D. Tang, "Self-assembled topological insulator: Bi_2Se_3 membrane as a passive Q-switcher in an erbium-doped fiber laser," J. Lightwave Technol. **31**, 2857–2863 (2013).
6. H. O. Churchill and P. Jarillo-Herrero, "Phosphorus joins the family," Nat. Nanotechnol. **9**, 330–331 (2014).
7. Y. Xu, Z. Wang, Z. Guo, H. Huang, Q. Xiao, H. Zhang, and X. Yu, "Solvothermal synthesis and ultrafast photonics of black phosphorus quantum dots," Adv. Opt. Mater. **4**, 1223–1229 (2016).
8. J. Ma, S. Lu, Z. Guo, X. Xu, H. Zhang, D. Tang, and D. Fan, "Few-layer black phosphorus based saturable absorber mirror for pulsed solid-state lasers," Opt. Express **23**, 22643–22648 (2015).
9. L. Kong, Z. Qin, G. Xie, Z. Guo, H. Zhang, P. Yuan, and L. Qian, "Black phosphorus as broadband saturable absorber for pulsed lasers from 1 μm to 2.7 μm wavelength," Laser Phys. Lett. **13**, 045801 (2016).
10. Y. Chen, G. Jiang, S. Chen, Z. Guo, X. Yu, C. Zhao, H. Zhang, Q. Bao, S. Wen, D. Tang, and D. Fan, "Mechanically exfoliated black phosphorus as a new saturable absorber for both Q-switching and mode-locking laser operation," Opt. Express **23**, 12823–12833 (2015).
11. K. F. Mak, C. Lee, J. Hone, J. Shan, and T. F. Heinz, "Atomically thin MoS_2: a new direct-gap semiconductor," Phys. Rev. Lett. **105**, 136805 (2010).
12. Y. Jiang, L. Miao, G. Jiang, Y. Chen, X. Qi, X. Jiang, H. Zhang, and S. Wen, "Broadband and enhanced nonlinear optical response of MoS_2/graphene nanocomposites for ultrafast photonics applications," Sci. Rep. **5**, 16372 (2015).
13. A. A. Balandin, S. Ghosh, W. Bao, I. Calizo, D. Teweldebrhan, F. Miao, and C. N. Lau, "Superior thermal conductivity of single-layer graphene," Nano Lett. **8**, 902–907 (2008).
14. G. X. Ni, H. Z. Yang, W. Ji, S. J. Baeck, C. T. Toh, J. H. Ahn, B. Özyilmaz, G. X. Ni, H. Z. Yang, and W. Ji, "Tuning optical conductivity of large-scale CVD graphene by strain engineering," Adv. Mater. **26**, 1081–1086 (2014).
15. J. A. Wilson and A. D. Yoffe, "The transition metal dichalcogenides discussion and interpretation of the observed optical, electrical and structural properties," Adv. Phys. **18**, 193–335 (1969).
16. L. Sun, Z. Lin, J. Peng, J. Weng, Y. Huang, and Z. Luo, "Preparation of few-layer bismuth selenide by liquid-phase-exfoliation and its optical absorption properties," Sci. Rep. **4**, 4794 (2014).
17. S. B. Lu, C. J. Zhao, Y. H. Zou, S. Q. Chen, Y. Chen, Y. Li, H. Zhang, S. C. Wen, and D. Y. Tang, "Third order nonlinear optical property of Bi_2Se_3," Opt. Express **21**, 2072–2082 (2013).
18. M. W. Lin, C. Ling, Y. Y. Zhang, H. J. Yoon, M. C. Cheng, L. A. Agapito, N. Kioussis, N. Widjaja, and Z. X. Zhou, "Room-temperature high on/off ratio in suspended graphene nanoribbon field-effect transistors," Nanotechnology **22**, 265201 (2011).
19. X. Li, X. Wang, L. Zhang, S. Lee, and H. Dai, "Chemically derived, ultrasmooth graphene nanoribbon semiconductors," Science **319**, 1229–1232 (2008).
20. Y. Zhang, J. Ye, Y. Matsuhashi, and Y. Iwasa, "Ambipolar MoS_2 thin flake transistors," Nano Lett. **12**, 1136–1140 (2012).
21. H. Zhu, C. A. Richter, E. Zhao, J. E. Bonevich, W. A. Kimes, H. J. Jang, H. Yuan, H. T. Li, A. Arab, O. Kivillov, J. E. Maslar, D. E. Ioannou, and Q. L. Li, "Topological insulator Bi_2Se_3 nanowire high performance field-effect transistors," Sci. Rep. **3**, 1757 (2013).
22. Q. L. Bao, H. Zhang, Y. Wang, Z. Ni, Y. Yan, Z. X. Shen, K. P. Loh, and D. Y. Tang, "Atomic-layer graphene as a saturable absorber for ultrafast pulsed lasers," Adv. Funct. Mater. **19**, 3077–3083 (2009).
23. H. Zhang, Q. L. Bao, D. Y. Tang, L. M. Zhao, and K. P. Loh, "Large energy soliton erbium-doped fiber laser with a graphene-polymer composite mode locker," Appl. Phys. Lett. **95**, 141103 (2009).
24. J. Du, Q. K. Wang, G. B. Jiang, C. W. Xu, C. J. Zhao, Y. J. Xiang, Y. Chen, S. C. Wen, and H. Zhang, "Ytterbium-doped fiber laser passively mode locked by few-layer molybdenum disulfide (MoS_2) saturable absorber functioned with evanescent field interaction," Sci. Rep. **4**, 6346 (2014).
25. H. Zhang, S. B. Lu, J. Zheng, J. Du, S. C. Wen, D. Y. Tang, and K. P. Loh, "Molybdenum disulfide (MoS_2) as a broadband saturable absorber for ultra-fast photonics," Opt. Express **22**, 7249–7260 (2014).
26. Z. Q. Luo, Y. Z. Huang, J. Weng, H. H. Cheng, Z. Q. Lin, B. Xu, Z. P. Cai, and H. Y. Xu, "1.06 μm Q-switched ytterbium-doped fiber laser using few-layer topological insulator Bi_2Se_3 as a saturable absorber," Opt. Express **21**, 29516–29522 (2013).

27. H. Mu, Z. Wang, J. Yuan, S. Xiao, C. Chen, Y. Chen, Y. Chen, J. Song, Y. Wang, Y. Xue, H. Zhang, and Q. Bao, "Graphene-Bi_2Te_3 heterostructure as saturable absorber for short pulse generation," ACS Photon. **2**, 832–841 (2015).
28. J. S. Ponraj, Z. Xu, S. C. Dhanabalan, H. Mu, Y. Wang, J. Yuan, P. Li, S. Thakur, M. Ashrafi, K. Mccoubrey, Y. Zhang, S. Li, H. Zhang, and Q. Bao, "Photonics and optoelectronics of two-dimensional materials beyond graphene," Nanotechnology **27**, 462001 (2016).
29. M. Z. Rahman, C. W. Kwong, K. Davey, and S. Z. Qiao, "2D phosphorene as a water splitting photocatalyst: fundamentals to applications," Energy Environ. Sci. **9**, 709–728 (2016).
30. H. Tian, M. L. Chin, S. Najmaei, Q. Guo, F. Xia, H. Wang, and M. Dubey, "Optoelectronic devices based on two-dimensional transition metal dichalcogenides," Nano Res. **9**, 1543–1560 (2016).
31. Q. H. Wang, K. Kalantar-Zadeh, A. Kis, J. N. Coleman, and M. S. Strano, "Electronics and optoelectronics of two-dimensional transition metal dichalcogenides," Nat. Nanotechnol. **7**, 699–712 (2012).
32. Y. C. Lin, H. P. Komsa, C. H. Yeh, T. Björkman, Z. Y. Liang, C. H. Ho, Y. S. Huang, P. W. Chiu, A. V. Krasheninnikov, and K. Suenaga, "Single-layer ReS_2: two-dimensional semiconductor with tunable in-plane anisotropy," ACS Nano **9**, 11249–11257 (2015),.
33. E. Gibney, "The super materials that could trump graphene," Nature **522**, 274–276 (2015).
34. L. Hart, S. Dale, S. Hoye, J. L. Webb, and D. Wolverson, "Rhenium dichalcogenides: layered semiconductors with two vertical orientations," Nano Lett. **16**, 1381–1386 (2016).
35. D. Wolverson and L. S. Hart, "Lattice dynamics of the rhenium and technetium dichalcogenides," Nano. Res. Lett. **11**, 250 (2016).
36. M. Rahman, K. Davey, and S. Z. Qiao, "Advent of 2D rhenium disulfide (ReS_2): fundamentals to applications," Adv. Funct. Mater. **27**, 1606129 (2017).
37. E. Liu, Y. Fu, Y. Wang, Y. Feng, H. Liu, X. Wan, W. Zhou, B. Wang, L. Shao, C. H. Ho, Y. S. Huang, Z. Cao, L. Wang, A. Li, J. Zeng, F. Song, X. Wang, Y. Shi, H. Yuan, H. Y. Hwang, Y. Cui, F. Miao, and D. Xing, "Integrated digital inverters based on two-dimensional anisotropic ReS_2 field-effect transistors," Nat. Commun. **6**, 6991 (2015).
38. S. Tongay, H. Sahin, C. Ko, A. Luce, W. Fan, K. Liu, J. Zhou, Y. S. Huang, C. H. Ho, J. Yan, D. F. Ogletree, S. Aloni, J. Ji, S. Li, J. Li, F. M. Peeters, and J. Wu, "Monolayer behavior in bulk ReS_2 due to electronic and vibrational decoupling," Nat. Commun. **5**, 3252 (2014).
39. O. Madelung, *Introduction to Solid-State Theory*, M. Cardona, P. Fulde, K. V. Klitzing, and H. Queisser, eds. (Springer, 1996), Vol. **2**.
40. F. Banhart, J. Kotakoski, and A. V. Krashennikov, "Structural defects in graphene," ACS Nano **5**, 26–41 (2010).
41. S. X. Wang, H. H. Yu, H. J. Zhang, A. Z. Wang, M. W. Zhao, Y. X. Chen, L. M. Mei, and J. Y. Wang, "Broadband few-layer MoS_2 saturable absorbers," Adv. Mater. **26**, 3538–3544 (2014).
42. T. Li and G. Galli, "Electronic properties of MoS_2 nanoparticles," J. Phys. Chem. C **111**, 16192–16196 (2007).
43. Y. D. Cui, F. F. Lu, and X. M. Liu, "Nonlinear saturable and polarization-induced absorption of rhenium disulphide," Sci. Rep. **7**, 40080 (2017).
44. D. Mao, X. Q. Cui, X. T. Gan, M. K. Li, W. D. Zhang, H. Lu, and J. L. Zhao, "Passively Q-switched and mode-locked fiber laser based on a ReS_2 saturable absorber," IEEE J. Sel. Top. Quantum Electron. **24**, 1100406 (2018).
45. X. C. Su, H. K. Nie, Y. R. Wang, G. R. Li, B. Z. Yan, B. T. Zhang, K. J. Yang, and J. L. He, "Few-layered ReS_2 as saturable absorber for 2.8 μm solid state laser," Opt. Lett. **42**, 3502–3505 (2017).
46. Z. G. Yu, Y. Q. Cai, and Y. W. Zhang, "Robust direct bandgap characteristics of one- and two-dimensional ReS_2," Sci. Rep. **5**, 13783 (2015).
47. C. H. Ho, Y. S. Huang, P. C. Liao, and K. K. Tiong, "Crystal structure and band-edge transitions of $ReS_{2-x}Se_x$ layered compounds," J. Phys. Chem. Solids **60**, 1797–1804 (1999).
48. D. Mao, S. L. Zhang, Y. D. Wang, X. T. Gan, W. D. Zhang, T. Mei, Y. G. Wang, Y. S. Wang, H. B. Zeng, and J. L. Zhao, "WS_2 saturable absorber for dissipative soliton mode locking at 1.06 and 1.55 μm," Opt. Express **23**, 27509–27519 (2015).
49. S. Tongay, J. Suh, C. Ataca, W. Fan, A. Luce, J. S. Kang, J. Liu, C. Ko, R. Raghunathanan, J. Zhou, F. Ogletree, J. Li, J. C. Grossman, and J. Wu, "Two-dimensional semiconductor alloys: Monolayer $Mo_{1-x}W_xSe_2$," Sci. Rep. **3**, 2657 (2014).
50. D. A. Chenet, O. B. Aslan, P. Y. Huang, C. Fan, A. M. van der Zande, T. F. Heinz, and J. C. Hone, "In-plane anisotropy in mono- and few-layer ReS_2 probed by Raman spectroscopy and scanning transmission electron microscopy," Nano Lett. **15**, 5667–5672 (2015).
51. Y. Feng, W. Zhou, Y. Wang, J. Zhou, E. Liu, Y. Fu, Z. Ni, X. Wu, H. Yuan, F. Miao, B. Wang, X. Wan, and D. Xing, "Raman vibrational spectra of bulk to monolayer ReS_2 with lower symmetry," Phys. Rev. B **92**, 054110 (2015).
52. M. Sheik-Bahae, A. A. Said, T. H. Wei, D. J. Hagan, and E. W. Van Stryland, "Sensitive measurement of optical nonlinearities using a single beam," IEEE J. Quantum Electron. **26**, 760–769 (1990).
53. Y. F. Chen and Y. P. Lan, "Comparison between c-cut and a-cut Nd: YVO_4 lasers passively Q-switched with a Cr^{4+}: YAG saturable absorber," Appl. Phys. B **74**, 415–418 (2002).
54. P. Sévillano, P. Georges, F. Druon, D. Descamps, and E. Cormier, "32-fs Kerr-lens mode-locked Yb:$CaGdAlO_4$ oscillator optical pumped by a bright fiber laser," Opt. Lett. **39**, 6001–6004 (2014).